# Effects of Substrates on Structural and Morphological Characteristics of Radio Frequency Sputtered ZnO Layers

**Omar Hamad Alzobaedy[1], Noor Najmuldeen[2], A.A. Salim[3], H. Bakhtiar[4*]**

## Abstract

High quality Zinc Oxide nanostructures (ZONSs) with customized traits became demanding for diverse applications. Based on this fact, some ZONSs with varied layer thicknesses (100 to 400 nm) were deposited on three types of Si (plain, polished and etched) and borosilicate glass substrates using the radio frequency (RF) sputtering method. As-deposited samples were characterized systematically using various techniques to determine the effects of the substrates on their structures and morphologies. The XRD analyses of the sample showed the formation of high quality nanocrystallites with varying sizes where the crystallinity was improved with the increase of layer thickness and change of substrates. The FESEM and AFM images exhibited the nucleation of dense nanocrystallites with some pores/voids with enhanced surface roughness. In addition, the EDX spectra displayed the presence of appropriate chemical elements in the ZONSs layers. Sample grown on the etched Si substrate at layer thickness of 300 nm was found to be optimum. The results for the etched Si were presented. It was demonstrated that by optimizing the RF sputtering parameters (power of 100 W, Argon flow of 10 sccm and pressure of 10-5 mb) the structural and morphological traits of the layered ZONSs can be tailored. The proposed ZONSs may be useful for various optoelectronic applications including the metal-semiconductor-metal (MSM) ultraviolet (UV) photodetectors fabrication.



**Key Words:** RF Sputtering, Substrate, ZONSs, Structure, Morphology.

**DOI Number: 10.14704/nq.2021.19.6.NQ21073** **NeuroQuantology 2021; 19(6):90-97**

## Introduction

The n-type Zinc Oxide (ZnO) material with wide band gap energy (3.3 eV), outstanding electrical and optical properties is a gifted semiconductor for diverse applications. The ZnO thin layers (ZTLs) with lattice direction along the crystallographic c-axis have intensively been used for acoustic wave detection (Cheong *et al,* 2002). The metallic nanoparticles (NPs)-doped ZTLs have widely been inspected to make efficient transparent conducting electrodes (Ohyama *et al,* 1998). Recently, the room temperature UV and visible photoluminescence (PL) emission from ZTLs became promising for the fabrication of efficient diode lasers (Salim *et al,* 2018; Van Veen *et al,* 2003) and phosphors for the flat panel display (Alkahlout, 2015). It is known that the electronic properties of ZTLs are significantly influenced by their composition, crystal structures, and phases.

**Corresponding author:** H. Bakhtiar

**Address:** [1]Laser Center & Physics Department, Faculty of Science, Universiti Teknologi; [2]Laser Center & Physics Department, Faculty of Science, Universiti Teknologi; [3]Laser Center & Physics Department, Faculty of Science, Universiti Teknologi; [4*]Laser Center & Physics Department, Faculty of Science, Universiti Teknologi.

[4*]E-mail: hazri@utm.my

**Relevant conflicts of interest/financial disclosures:** The authors declare that the research was conducted in the absence of any commercial or financial relationships that could be construed as a potential conflict of interest.

**Received:** 02 April 2021 **Accepted:** 18 May 2021

The high electrical conductivity shown by the pure and doped ZTLs was attributed to the presence of O vacancy and Zn interstitial as well as the high quality polycrystalline character with strong lattice orientation (Yao, 2009). The green and orange PL obtained from the ZTLs was ascribed to the generation of respective oxygen-poor and oxygen-rich structures (Minami, 2005).

Over the years, various methods have been developed to get optimum chemical compositions, crystalline structures and desired morphology of ZTLs in a customized way (Minami, 2005; Salim *et al,* 2020; Kahlout *et al,* 2014; Alkaim, A.F. 2017). In addition, the nanostructured ZTLs also called ZnO nanofilms became prospective substitute to the GaN-based UV photodetectors as an absorption layer (AlKahlout, 2013). Generally, the ZTLs are synthesized by solution-based processing, sol–gel and various vacuum deposition techniques. The radio frequency (RF) sputtering and pulsed-laser deposition (PLD) methods are favored to grow good quality layer by layer nanocrystallites of various semiconductors. The RF sputtering can also be used to get direct pattern of the conducting- and semiconducting- oxide electrodes for high performance optoelectronic applications (Fortunato *et al,* 2008). Moreover, compared to the sputtering method the deposition of ZTLs by solution-based methods is limited due to poor structural quality and finer grain sizes with broad size distributions (Agura *et al,* 2003). Thus, the ZTLs deposited by the RF sputtering method can achieve excellent structural, morphological, electrical, and optical properties which are advantageous for many practical device applications. On top, RF sputterd ZTLs is very useful due to area selective rapid crystallization without the need of high temperature heating, thus leading to minimal disorder in the adjacent structural regions (Ohta *et al,* 2000; Kuroyanagi *et al,* 1989; Marie *et al,* 2008; salim *et al,* 2021; Groenen *et al,* 2001).

Considering the basic and applied significance of the ZTLs, we deposited some layered ZnO nanostructures of different thicknesses (100 to 400 nm) on various substrates such as plain Si, polished Si, etched Si and borosilicate glass via the RF sputtering approach. As-prepared ZONSs were analyzed using X-ray diffraction, filed emission scanning electron microscopy (FESEM), atomic force microscopy and energy dispersive X-ray (EDX) spectroscopy measurements. The impact of different substrates and layer thickness on the structures and morphologies of the studied ZONSs were evaluated. Results were analyzed, discussed, interpreted and compared with other existing state-of-the-art reports.

## Materials and Methods

A series nanostructured ZTLs were deposited (at a rate of 0.3 A°/sec) on three types (plain, polished and etched) of n-type Si (100) substrates (each dimension 2.5 cm × 2.5 cm) using the standard RF magnetron sputtering technique (at 300 °C, RF power of 100 W and Argon flow of 10 sccm and pressure of $10^{-5}$ mb). All the substrates were first cleaned for 15 min in Decon 90 surfactant solutions to eliminate the surface contaminants and then washed in de-ionized water to remove the surface impostures and ions (Nishino *et al,* 1997). The presence of surface contaminants is known to cause poor adhesion of the deposited thin film layers, producing pinholes on the surface of the thin films (Shim *et al,* 2002). Next, the cleaned substrates were dried in the oven (at 150 °C) for 25 min to diffuse the residual water or solvent exist on the surface. The polycrystalline ZONSs were grown using a ZnO target (99.999% purity). Prior to the deposition, the target was sputtered cleaned for 10 min to remove any contaminants and differential sputtering effect. The thickness of the ZONSs layers were controlled by the thin film analyzer (Filmetrics F20, USA) and deposition time. The morphological and structural properties of as-deposited samples were characterized using the X-ray diffractometer (Bruker D8 Advance Diffractometer operated with Cu-K$\alpha_1$ radiation wavelength of 1.540 A° at 40 kV and 100 mA). The angular scanning range (2θ) was varied from 20-75°. A slow speed of scanning (~ 1.2°/min) at a resolution of 0.011° was use to record the XRD patterns. The elemental composition of sample was analyzed through energy dispersive X-ray (EDX) spectroscopy attached to FESEM (JEOL, JSM-6701F). The surface topography of the samples was imaged using the atomic force microscopy (AFM, Seiko Instruments, SPA-300HV).

## Results and Discussion

Figure 1 shows the XRD patterns of ZONSs of various thickness (100, 200, 300 and 400 nm) deposited on etched Si substrate (left) and the corresponding Gaussian fit of the major peak with FWHM (right). Irrespective of the ZONSs layer thickness, all the XRD profile displayed two

prominent diffraction peaks of ZnO due to the lattice planer orientation of (002) and (101), indicating the good crystallinity of the film. In addition, the sharp peak corresponding to the Si substrate was also observed. Interestingly, the intensities of the XRD peaks became sharper for the ZONSs deposited on etched Si substrate than those grown on other substrates, indicating the strong influence of substrate together with the layer thickness. Samples with the thickness of 100, 200, 300 and 400 nm revealed the most intense (002) Bragg's diffraction peaks at the 2θ values of 34.42503, 34.43198, 34.43519 and 34.40559$^{o}$ with the corresponding FWHM of 0.25601, 0.39304, 0.30921 and 0.29788$^{o}$, respectively (Table 4.3). The increase in the FWHM values with the increase of layer thickness clearly indicated a decrease in the nanocrystallite size in the film (from 32.48736632 nm for 100 nm layer thickness to 27.91838604 nm for 400 nm layer thickness). This observation was attributed to the effect of quantum confinement of the ZONSs. Sample prepared with layer thickness of 400 nm exhibited the most intense diffraction peak, indicating the high crystalline quality of the film.

The differences in the intensities of the peaks were mainly due to the irregularities in the lattice planer orientations together with the values of miller indices (hkl). The weaker diffraction at (101) indicated the weaker growth orientation along this lattice plane. However, the intensity of the (101) peak for the ZONSs deposited on polished Si substrate became stronger compared to the one deposited on other substrates. The growth orientation variation along the preferred direction might have some effects on the XRD intensities thus leading to the X-ray scattering changes from the crystal components and/or their lattice arrangements. The morphologies (shapes, nanocrystallite density, size distribution, and sizes) of the ZONSs were varied significantly with the layer thickness variations as clearly reflected in the XRD patterns. The impact of different layer thickness on the ZONSs morphologies was determined by estimating the mean grain size as shown in Table (Shim *et al,* 2002). The most intense XRD peak (002) was fitted with the Gaussian to calculate the crystallite size (D) in the film using the Debye-Scherrer formula and presented in Table.

The ZONSs deposited with layer thickness of 100 nm showed the largest average crystallite size of 32.48736632 nm and the one deposited with layer thickness of 200 nm showed the smallest average crystallite size of 21.16049781nm. The ZONSs deposited with layer thickness of 300 nm and 400 nm displayed the average crystallite size of 26.89755911 nm and 27.91838604 nm, respectively. This sudden decrease in the crystallite size at 200 nm layer thickness and then increase at 300 nm thickness may be due to the generation of some extra microstrain and defects in the film. Overall, the crystallinity of the film was improved as the mean grain size was decreased which was indicated by the increase in the XRD intensity. Briefly, the improvement in the XRD intensity with the increase in layer thickness and reduction in the mean crystallite size verified an enhancement in the nanocrystallinity of the ZONSs film. This observation of the reduction in crystalline size with the increase in layer thickness clearly signified the sample crystallinity enhancement and more packing or high density ZONSs. The enhancement in the FWHM, crystallinity and density of NSs (shrinkage in the nanocrystallite sizes) was indeed caused by quantum size effect (confinement due to crystalline size reduction). These observations were consistent with the similar findings reported in the literature (Kuroyanagi *et al,* 1989; Al-Hussain *et. al.* 2017). Considering the higher crystallinity and small crystallite size in the ZONSs deposited with the layer thickness of 300 nm (high quality film) this film was selected as the optimum one.



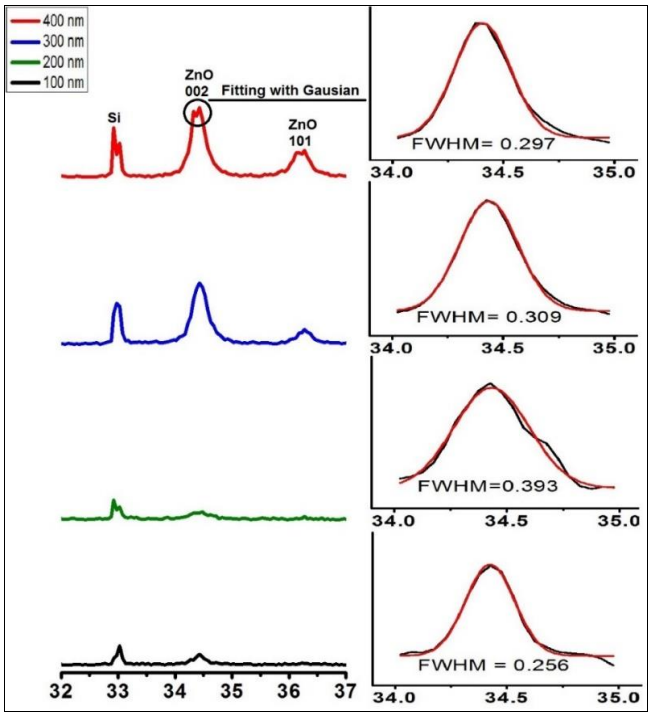


**Figure 1.** XRD Patterns of ZONSs of various thickness deposited on etched Si substrate (left) and the corresponding Gaussian fit of the major peak with FWHM (right)

**Table 1.** Thickness-dependent XRD peak positions, FWHM, and nanocrystallite sizes of ZONSs deposited on etched Si substrate.

| Thickness (nm) | Peak Position (Deg.) | FWHM (Deg.) | Crystallite Size, D (nm) |
|---|---|---|---|
| 100 | 34.42503 | 0.25601 | 32.48736632 |
| 200 | 34.43198 | 0.39304 | 21.16049781 |
| 300 | 34.43519 | 0.30921 | 26.89755911 |
| 400 | 34.40559 | 0.29788 | 27.91838604 |

Figure 2 illustrates the EDX spectra of ZONSs of various thickness (100, 200, 300 and 400 nm) deposited on etched Si substrate. All the EDX spectra correctly detected the weight percentages of oxygen (O), Zn and Si. In addition, the intensity corresponding to the Zn and O peaks became stronger and Si peak became weaker with the increase of ZONSs layer thickness, indicating the achievement of enhanced crystallinity and high density structures. This observation is supported by the XRD results that showed the increase in crystallinity in the samples with the increase in ZONSs layer thickness. The ZONSs deposited with the layer thickness of 400 nm showed the maximum elemental contents of both Zn and O. The compositions of the nanofilms deposited with different was evaluated in terms of the Zn and O stoichiometric ratio where right amount of Zn, O, and Si were detected in the sample. Some reported literature stated that the optimum ZnO layers show an ideal stoichiometric ratio between Zn and O approximately 60% (Shim *et al,* 2002; Nunes *et al,* 1999).

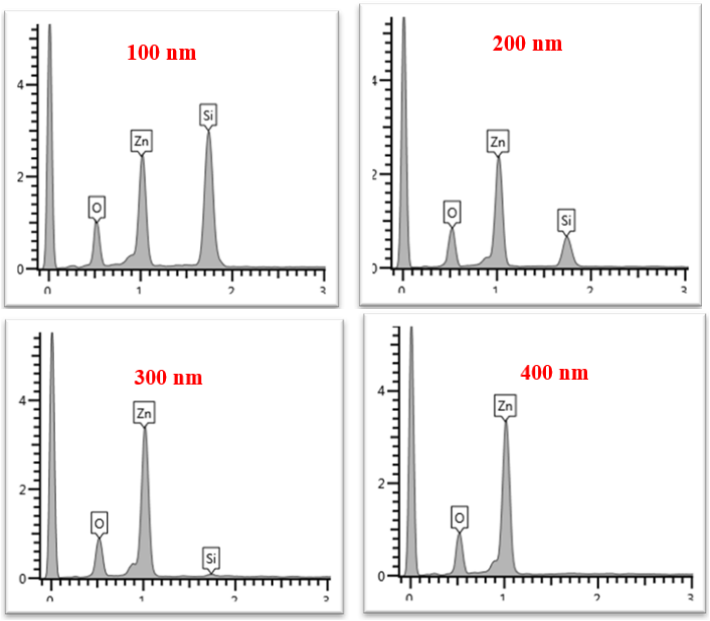


**Figure 2.** EDX spectra of ZONSs of various thicknesses deposited on etched Si substrate

Figure 3 displays the FESEM cross-sectional images of ZONSs of various thickness (100, 200, 300 and 400 nm) deposited on the etched Si substrate. All the as-prepared samples (especially with 100 and 200 nm of layer thicknesses) showed very weakly cracked ZnO layers formation with almost smooth surface, tiny crystallites, very narrow and asymmetric voids/pores/defects among them. In addition, the size of the crystallites was very tiny at lower layer thicknesses. The morphology of the films deposited at layer thicknesses of 100 and 200 nm on the etched Si substrate was very different from the one deposited on other substrates. Higher degree of partially cracked and nonparallel ZnO walls of length of below 5 µm was displayed by the sample with 100 and 200 nm layer thicknesses (Fu *et al,* 2002; Abbas *et al,* 2016; Permana *et al,* 2017). The samples with 300 and 400 nm layer thicknesses revealed enhanced crystalline quality, where the flakes and leaves like nanocrystals with very higher density and much bigger sizes were nucleated. Sample synthesized with the layer thickness of 400 showed larger crystallites size with higher density, regularity and close packing (less defects and cracks) than the one obtained with 300 nm of layer thicknesses. Clearly, these results are consistent with the XRD data.

It is argued that the strain on the whole film surface was developed with the increase in thickness of the film, improving the crystal quality and enhanced

morphology and surface roughness (revealed AFM analyses). The sample with thickness of 300 nm exhibited considerably wider voids/pores across the entire surface which became irregular with thicknesses up to 10 $\mu$m (smaller than those nucleated on the normal Si substrate). At the layer thickness of 400 nm much bigger irregular voids/defects were formed than the film deposited at 300 nm. On top, these walls and defects/pores/voids became more regular with larger dimension at 400 nm of layer thickness, indicating an enhanced crystalline density and smaller grain sizes with narrow particles size distribution suitable for UV photodetectors applications. In short, an increase in the layer thicknesses of the ZONSs strongly affected the morphology, structure and crystalline quality of the deposited films.

It is important to mention that the ZONSs films surface showed some voids/pores/defects and these voids were distributed randomly and appeared elongated and flakes-like with the increase in the layer thickness. With the increase in the layer thickness, these voids/pores became more apparent and oriented in certain direction. This observation well agreed with the XRD peak intensification at higher layer thickness. Besides, the ZnO grain size, particle size distribution, crystalline density, and morphologies of the films were evolved depending on the layer thickness. This confirmed the impact of the layer thickness on the pores/voids shapes and sizes. The evolution of the ZnO nanocrystals with regular flakes/leaves (somewhat like nanoislands) in the presence of pores/defects indicated the free energy minimization process in the structure. At lower layer thickness (100 and 200 nm), fewer voids/pores were observed. Sample grown at higher layer thickness (300 and 400 nm), the flakes/leaves-like structure, and uniformity across the whole surface of the substrate was enhanced. The growth mechanism was ascribed to the combined influence of Stranski–Krastanov (S-K) and Volmer-Weber (V–W) modes (Permana *et al,* 2017; Tang *et al,* 1994; Abbas *et al,* 2021).

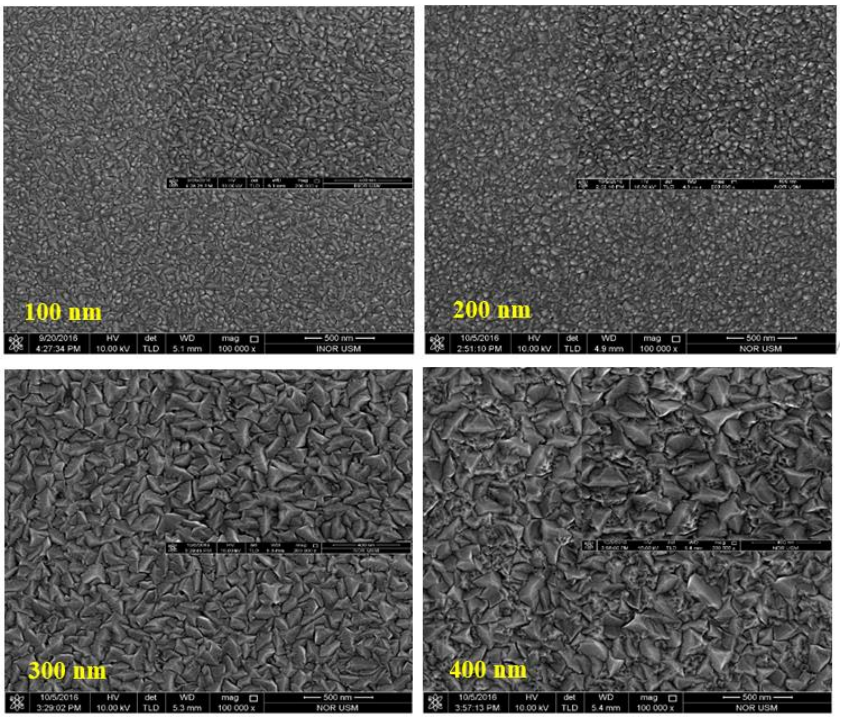


**Figure 3.** FESEM images of ZONSs of various thickness deposited on etched Si substrate

Figure 4 presents the AFM images (3D view) of ZONSs of various thickness (100, 200, 300 and 400 nm) deposited on the etched Si substrate (inset shows the surface roughness over scan length on the film). Irrespective of the layer thickness variation, all the film showed the nucleation of ZnO nanocrystallites with different morphology and surface roughness. All the as-prepared samples (especially with 100 and 200 nm of layer thicknesses) showed tinier particles size distribution with rough surface, irregular ridges, tiny crystallites, very narrow and asymmetric

voids. In addition, the size of the crystallites was very tiny at lower layer thicknesses. The morphology of the films deposited at layer thicknesses of 100 and 200 nm on the etched Si substrate was very different from the one deposited on other substrates, indicating the role of substrate on the growth evolution of the ZONSs. Furthermore, the surface became more regular with the increase in layer thickness. The highest surface roughness (rms) was estimated to be approximately 220 nm. In addition, ZONSs deposited with 300 nm of layer thickness disclosed lower surface roughness of the ZnO (root mean square value of about 360 nm over the scan area of $5 \times 5$ μm$^2$) compared to the sample prepared at layer thickness of 400 nm (root mean square value of 325 nm). This indicated the preferred use of etched Si substrate to deposit ZONSs at different layer thickness (Salim *et al,* 2017; Horng *et al,* 2016; Wei *et al,* 2011). Due to the attainment of the larger crystallite size and enhanced roughness, mobility of the electron can increase, thus leading to higher photodetector sensitivity and responsivity. These results are consistent with the FESEM and XRD data analyses.

The achievement of relatively lower porosity/defects/voids and larger crystallite size with more irregular and dense morphology of the deposited ZONSs at higher layer thicknesses compared to those deposited at lower layer thickness accounted for the increase in rms roughness. The rms surface roughness of the deposited nanofilm is very important for the high performance MSM UV photodetector applications because it is a measure of the surface textures and characterized by the vertical departure of a real surface from its ideal form. Briefly, the roughness value of the RF sputtered ZONSs were greatly affected by the layer thickness, indicating their enhanced photo conversion efficiency and blue shift of the PL peaks. The S-K and Volmer-Weber (V–W) growth processes were responsible for the nucleation of the ZnO islands on the film surface [Islam *et al,* 2018; Luo *et al,* 2012; Salim *et al,* 2021; Hasanpoor *et al,* 2012; Salim *et al,* 2020). In addition, the samples prepared with the layer thickness of 300 and 400 nm (regular roughness distribution) was found to be suitable for the UV photodetector fabrication because of the presence of ZnO islands/flakes/gouges/tunnels/ crevasse with high rms surface roughness.



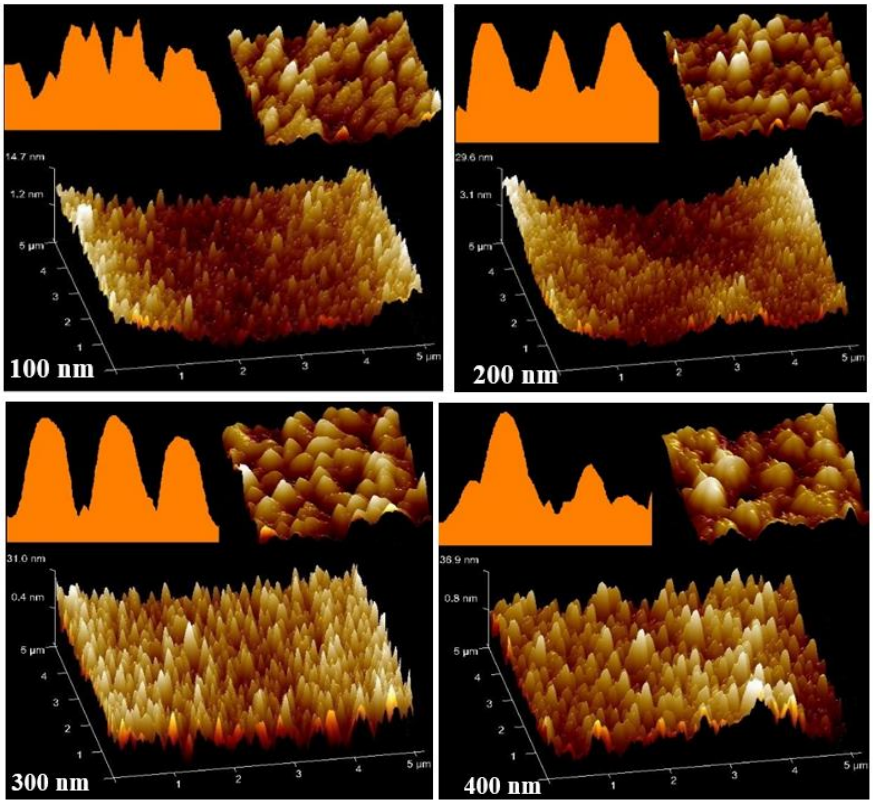


**Figure 4.** AFM images of ZONSs of various thicknesses deposited on etched Si substrate (inset shows the surface roughness over scan length on the film).

## Conclusion

This paper reported the structural and morphological characteristics of ZONSs with layer thicknesses of 100, 200, 300 and 400 nm deposited on different substrates via the conventional RF sputtering technique operated at optimum growth parameters. The nature of the substrates and layer thicknesses variation was found to play a significant role on the structures and morphologies of the achieved ZONSs. The properties of the ZONSs deposited on the etched Si were presented here. The XRD patterns, FESEM and AFM micrographs of the as-deposited samples verified the formation of high quality ZnO nanocrystallites with varying grain sizes, grain distributions and surface roughness. Amongst all the studied layer thicknesses and substrates, ZONSs layer of thickness 300 nm deposited on the etched Si substrate was the best. It was concluded that by selecting the appropriate substrate, controlling the ZONSs layer thickness and optimizing the growth parameters the overall properties of the proposed ZONSs can be customized. The obtained optimum ZONSs deposited on the etched Si substrate with desirable properties may be beneficial for the development of diverse devices.

## Acknowledgements

Researcher are thankful to the Universiti Teknologi Malaysia (UTM), RMC and MOHE for the research financial support under the grants FRGS 04E86 and UTMFR 20H65.

## References

Abbas AM, Abid MA, Abbas KN, Aziz WJ, Salim AA. Photocatalytic activity of Ag-ZnO nanocomposites integrated essential ginger oil fabricated by green synthesis method. *Journal of Physics: Conference Series* 2021; 1892: 012005.

Abbas KN, Bidin N, Sabry RS, Al-Asedy HJ, Al-Azawi MA, Islam S. Structures and emission features of high-density ZnO micro/nanostructure grown by an easy hydrothermal method. *Materials Chemistry and Physics* 2016; 182: 298-307.

Agura H, Suzuki A, Matsushita T, Aoki T, Okuda M. Low resistivity transparent conducting Al-doped ZnO films prepared by pulsed laser deposition. *Thin Solid Films* 2003; 445(2): 263-267.

Al-Hussain AJA, Abd FG, Alkaim AF, Al-Azzawi A. Eco friendly synthesis, characterization and antibacterial activity of ZnO nanoparticles using bacillus subtilis against multi-drug resistant bacteria. *Journal of Global Pharma Technology* 2017; 9(7): 207-213.

AlKahlout A. A wet chemical preparation of transparent conducting thin films of Ga-doped ZnO nanoparticles. *Journal of Sol-Gel Science and Technology* 2013; 67(2): 331-338.

Alkahlout A. A comparative study of spin coated transparent conducting thin films of gallium and aluminum doped ZnO nanoparticles. *Physics Research International* 2015, 8.

Alkaim AF, Alrobayi EM, Algubili AM, Aljeboree AM. Synthesis, characterization, and photocatalytic activity of sonochemical/hydration–dehydration prepared ZnO rod-like architecture nano/microstructures assisted by a biotemplate: Environmental Technology (United Kingdom) 2017; 38 (17): 2119-2129.

Cheong KY, Muti N, Ramanan SR. Electrical and optical studies of ZnO: Ga thin films fabricated via the sol–gel technique. *Thin Solid Films* 2002; 410(1-2): 142-146.

Fortunato E, Raniero L Silva L Goncalves A Pimentel A Barquinha P Aguas H Pereira L Goncalves G Ferreira I, Elangovan E. Highly stable transparent and conducting gallium-doped zinc oxide thin films for photovoltaic applications. *Solar Energy Materials and Solar Cells* 2008; 92(12): 1605-1610.

Fu Z, Lin B, Zu J. Photoluminescence and structure of ZnO films deposited on Si substrates by metal-organic chemical vapor deposition. *Thin Solid Films* 2002; 402(1-2): 302-306.

Groenen R, Linden JL, Van Lierop HRM, Schram DC, Kuypers AD, Van De Sanden MCM. An expanding thermal plasma for deposition of surface textured ZnO: Al with focus on thin film solar cell applications. *Applied Surface Science* 2001; 173(1-2): 40-43.

Hasanpoor M, Aliofkhazraei M, Delavari H. Microwave-assisted synthesis of zinc oxide nanoparticles. *Procedia Materials Science* 2015; 11: 320-325.

Horng RH, Ou SL, Huang CY, Ravadgar P, Wu CI. Effects of Ga concentration and rapid thermal annealing on the structural, optoelectronic and photoluminescence properties of Ga-doped ZnO thin films. *Thin Solid Films* 2016; 605: 30-36.

Islam S, Bakhtiar H, Bidin N, Salim AA, Riaz S, Abbas KN, Naseem S. Influence of ZnO doping on structural, optical and pH-stimulus characteristics of silica-titania nanocomposite matrix. *Journal of Saudi Chemical Society* 2018; 22(7): 826-837.

Kahlout AA, Dahoudi NA, Heusing S, Moh K, Karos R, De Oliveira PW. Structural, electrical and optical properties of aluminum doped zinc oxide spin coated films made using different coating sols. *Nanoscience and Nanotechnology Letters* 2014; 6(1): 37-43.

Kuroyanagi A. Properties of aluminum-doped ZnO thin films grown by electron beam evaporation. *Japanese Journal of Applied Physics* 1989; 28(2R): 219.

Luo L, Rossell MD, Xie D, Erni R, Niederberger, M. Microwave-assisted nonaqueous sol–gel synthesis: from Al: ZnO nanoparticles to transparent conducting films. *ACS Sustainable Chemistry & Engineering* 2012; 1(1): 152-160.

Marie P, Portier X, Cardin J. Growth and characterization of gallium oxide thin films by radiofrequency magnetron sputtering. *Physica Status Solidi* 2008; 205(8): 1943-1946.

Minami T. Transparent conducting oxide semiconductors for transparent electrodes. *Semiconductor Science and Technology* 2005; 20(4): S35.

Nishino J, Kawarada T, Ohshio S, Saitoh H, Maruyama K, Kamata K. Conductive indium-doped zinc oxide films prepared by atmospheric-pressure chemical vapour



deposition. *Journal of Materials Science Letters* 1997; 16(8): 629-631.

Nunes P, Fernandes B Fortunato E, Vilarinho P, Martins R. Performances presented by zinc oxide thin films deposited by spray pyrolysis. *Thin Solid Films* 1999; 337(1-2): 176-179.

Ohta H, Orita M, Hirano M, Tanji, H Kawazoe, H, Hosono H. Highly electrically conductive indium–tin–oxide thin films epitaxially grown on yttria-stabilized zirconia (100) by pulsed-laser deposition. *Applied Physics Letters* 2000; 76(19): 2740-2742.

Ohyama M, Kozuka H, Yoko T. Sol-gel preparation of transparent and conductive aluminum-doped zinc oxide films with highly preferential crystal orientation. *Journal of the American Ceramic Society* 1998; 81(6): 1622-1632.

Permana AJ, Wulandari D, Hartati H, Setyawati H, Fahmi MZ. The Influence of pH Values on the Crystallite Size of ZnO by Solvothermal Synthesis. *Jurnal Kimia Riset* 2017; 2(2): 118-122.

Salim AA, Bakhtiar H, Bidin N, Ghoshal SK. Unique attributes of spherical cinnamon nanoparticles produced via PLAL technique: Synergy between methanol media and ablating laser wavelength. *Optical Materials* 2018; 85: 100-105.

Salim AA, Bakhtiar H, Krishnan G, Ghoshal SK. Nanosecond pulse laser-induced fabrication of gold and silver-integrated cinnamon shell structure: Tunable fluorescence dynamics and morphology. *Optics & Laser Technology* 2021; 138: 106834.

Salim AA, Bidin N, Lafi AS, Huyop FZ. Antibacterial activity of PLAL synthesized nanocinnamon. *Materials & Design* 2017; 132: 486-495.

Salim AA, Ghoshal SK, Bakhtiar H. Growth mechanism and optical characteristics of Nd: YAG laser ablated amorphous cinnamon nanoparticles produced in ethanol: Influence of accumulative pulse irradiation time variation. *Photonics and Nanostructures-Fundamentals and Applications* 2021; 43: 100889.

Salim AA, Ghoshal SK, Bakhtiar H. Tailored morphology, absorption and bactericidal traits of cinnamon nanocrystallites made via PLAL method: Role of altering laser fluence and solvent. *Optik* 2021; 226: 165879.

Salim AA, Ghoshal, SK, Krishnan G, Bakhtiar H. Tailored fluorescence traits of pulse laser ablated Gold-Cinnamon nanocomposites. *Materials Letters* 2020; 264: 127335.

Shim ES, Kang HS, Kang JS, Kim JH, Lee SY. Effect of the variation of film thickness on the structural and optical properties of ZnO thin films deposited on sapphire substrate using PLD. *Applied Surface Science* 2002; 186 (1-4): 474-476.

Tang W, Cameron DC. Aluminum-doped zinc oxide transparent conductors deposited by the sol-gel process. *Thin Solid Films* 1994; 238(1): 83-87.

Van Veen MK, Van der Werf CHM, Rath JK, Schropp REI. Incorporation of amorphous and microcrystalline silicon in n–i–p solar cells. *Thin Solid Films* 2003; 430(1-2): 216-219.

Wei H, Li M, Ye Z, Yang Z, Zhang Y. Novel Ga-doped ZnO nanocrystal ink: Synthesis and characterization. *Materials letters* 2011; 65(3): 427-429.

Yao T, Hong SK. Oxide and nitride semiconductors: Processing, properties, and applications. *Springer Science and Business Media* 2009: 12.

Farnia V, Alikhani M, Davarinejad O, Golshani S, Salemi S, Hookari S, Jalali A, Radmehr F, Ramyar H. A discriminant analysis of psychological and brain-behavioural system features to predict methamphetamine dependence. *NeuroQuantology* 2019; 17(8): 24-32.